Gravitational effects on the deformation of a droplet adhering to a horizontal solid surface in shear flow

P. Dimitrakopoulos
Department of Chemical and Biomolecular Engineering, University of Maryland, College Park, Maryland 20742, USA

(Received 12 February 2007; accepted 30 October 2007; published online 19 December 2007)

In this paper we investigate the gravitational effects on the deformation of a three-dimensional droplet adhering to a horizontal rough solid surface in steady shear Stokes flows. Our study considers both positive and negative Bond numbers for viscous and inviscid droplets. When the interfacial system is initially at hydrostatic equilibrium, our study shows that the Bond number affects the deformation of viscous droplets with moderate and large initial contact angles in a different way than those for small angles owing to the interplay between the viscous and surface tension forces. Inviscid droplets with different initial contact angles show similar behavior as the Bond number increases, i.e., their deformation is monotonically decreased owing to the monotonic decrease of the droplets' height and thus the exerted pressure force. Our study identifies the gravitational effects of the onset of interfacial sliding, i.e., on the portions of the contact line which slide first due to violation of the hysteresis condition. When the interfacial system is not at hydrostatic equilibrium at the flow initiation, its dynamic evolution is more complicated owing to the combined action of the shear flow with the gravitational forcing due to the difference between the initial shape with the hydrostatic one. Our computational results are accompanied with an analysis of the forces on the droplet which provides physical insight and identifies the three-dimensional nature of the interfacial deformation. © *2007 American Institute of Physics*.
[DOI: 10.1063/1.2821127]

I. INTRODUCTION

The deformation, sliding, and dislodging of fluid droplets adherent to solid substrates show applications in numerous areas including distillation, spray coating, packed towers, and a variety of multiphase flow operations in the chemical process industry. Our interest in the problem focuses on viscous flows at low Reynolds number. This regime has relevance in coating operations, enhanced oil recovery, microfluidics, and biological systems.[1–4]

The main characteristic of the interfacial attachment on rough and chemically inhomogeneous solid surfaces is the hysteresis effect where the contact line remains stationary as long as the contact angle θ satisfies the requirement

$$\theta_R \leq \theta \leq \theta_A \tag{1}$$

anywhere along the contact line. (The advancing and receding angles, θ_A and θ_R, are properties of the specific interfacial system.[5,6]) As a result, the entire process under external forcing (i.e., a shearing flow) may exhibit several stages including interfacial deformation with a stationary contact line, initial sliding with partial rearrangement of the contact line, and the final drop dislodging, depending on the strength of the external forcing.[7]

Several studies have considered the drop deformation under fixed constant line conditions for two- and three-dimensional interfaces at both low- and finite-Reynolds numbers, e.g., Refs. 8–12. Recently, Dimitrakopoulos[7] also considered the deformation of three-dimensional attached droplets with fixed circular contact lines but focused his interest on the onset of interfacial sliding under contact angle hysteresis. The fundamental issues associated with the yield criteria for drop displacement from rigid boundaries (i.e., the equilibrium conditions just before the final drop dislodging) have been addressed in a series of papers by Dussan and co-workers,[13–15] and by Dimitrakopoulos and Higdon.[5,6,16–18] The flow-induced droplet sliding has been considered by several computational studies mainly for systems with negligible contact angle hysteresis where even the slightest external forcing is able to cause interfacial sliding, e.g., Refs. 10, 12, 19, and 20.

We emphasize that the aforementioned studies commonly ignored the gravitational effects on the drop deformation and sliding by considering fluids with the same density or very small droplets where the Bond number can be neglected due to its stronger length dependence (compared to that for the capillary number) as seen in Eq. (2) below.

However, for many systems the gravitational effects cannot be neglected even for relatively small droplets. For example, a 10 μl drop having the surface tension of water and a density difference equal to the density of water, shows a Bond number $B_d \approx \pm 0.31$. The corresponding Bond numbers for 50 and 100 μl drops are $B_d \approx \pm 0.91$, 1.44. [We note that the aforementioned drop volumes exhibit a radius of $O(1\ \text{mm})$ when they acquire a spherical shape.] The hydrostatic shapes of these droplets attached to horizontal solid surfaces are thus much deformed compared to the spherical-cap shape of zero-Bond-number droplets. Therefore, the flow-induced deformation of such droplets may differ considerably from that for negligible Bond number.

In the present study we consider the gravitational effects

on the dynamics of a three-dimensional droplet attached to a horizontal rough plane wall with a stationary contact line in the presence of a steady shear flow at low Reynolds number. The initial shape of the drop is axisymmetric and thus, at the flow initiation, the drop forms a constant contact angle θ_0 (with $\theta_R \leq \theta_0 \leq \theta_A$) around a circular contact line. To study this problem, we employ our interfacial spectral boundary element algorithms described briefly in Sec. II. In particular, for the efficient determination of the droplet shape as a function of time, we employ our fully implicit time integration algorithm, while for the determination of the equilibrium deformation in a wide range of subcritical flow rates, we utilize our Newton method for equilibrium interfaces in Stokes flow. For the majority of our computations presented in Sec. III, the drops are at hydrostatic equilibrium for the desired Bond number at the instance of the flow initiation. This physical system may represent a droplet which has been attached to a solid surface under quiescent conditions, formed a (stationary) circular contact line, and acquired its hydrostatic shape for a given Bond number without violating the hysteresis condition, Eq. (1). Moreover, in Sec. III F we consider the case where a droplet may be attached to a solid surface without being at hydrostatic equilibrium at the flow initiation.

Our work includes both positive and negative Bond numbers for viscous and inviscid droplets, and identifies the gravitational effects on the drop deformation and dynamics for different initial configurations (i.e., different angles θ_0). Our computational results are accompanied with an analysis of the forces on the droplet interface which provide useful physical insight on the deformation behavior. We also identify the gravitational effects of the onset of interfacial sliding, i.e., on the portions of the contact line which slide first due to violation of the hysteresis condition, Eq. (1), in strong enough shear flows. As discussed in Sec. IV, our study identifies the three-dimensional nature of the deformation and sliding of adherent droplets owing to the ability of the drops to expand or contract in the cross-flow direction changing the interfacial dynamics.

Our interest lies on the interfacial deformation under a stationary contact line and the onset of interfacial sliding that occur at low and moderate flow rates. (Note that we do not consider interfacial breakup which may occur at high enough flow rates.) By considering representative values for small, moderate, and large initial angles and via the associated scaling analysis, the physical understanding presented in this work covers a wide range of contact angles for low and moderate flow rates.

As mentioned earlier, the physical system considered in this paper corresponds to the initial stage of the deformation/displacement process where the droplet deforms but its contact line remains stationary. This system provides physical insight for the droplet deformation and dynamics which is useful in processes where we want to keep the droplets attached to a solid surface. In addition, our work provides information on the onset of interfacial sliding. We emphasize that, for the problem studied in this paper, the onset of interfacial sliding cannot be inferred from the knowledge of the equilibrium contact angle distribution at gradually increasing flow rates. In particular, the interfacial sliding may occur during the transient evolution, depending on the flow rate, the physical parameters of the material system (i.e., θ_R, θ_A, the viscosity ratio and the Bond number) as well as the initial angle θ_0. As we discuss in Sec. III, the onset of interfacial sliding is strongly affected by the drop's initial configuration and the Bond number; this can be exploited to initiate interfacial sliding at a desired portion of the contact line.

II. MATHEMATICAL FORMULATION AND COMPUTATIONAL ALGORITHM

We consider a three-dimensional droplet attached to a horizontal plane solid wall surrounded by a viscous fluid [as shown later in Fig. 3(c)]. The droplet (fluid 1) has density ρ_1 and viscosity $\lambda\mu$, while the surrounding fluid (fluid 2) has density ρ_2 and viscosity μ. The droplet size is specified by its volume V or equivalently by the radius a of a spherical droplet of volume $4\pi a^3/3=V$. The gravitational acceleration is g while the surface tension γ is assumed constant. At time $t=0$, a steady shear flow $\boldsymbol{u}^\infty=(Gz,0,0)$, where G is the shear rate, is introduced into the system causing interfacial deformation. In our study the time is scaled with the flow time scale $\tau_f=G^{-1}$.

The dimensionless parameters which represent the strength of the viscous flow forces and the gravitational forces, with respect to the interfacial forces, are the capillary number Ca and Bond number B_d, respectively, defined by

$$\mathrm{Ca}=\frac{\mu \mathrm{Ga}}{\gamma}, \quad B_d=\frac{(\rho_1-\rho_2)ga^2}{\gamma}. \tag{2}$$

Note that the length scale a used in the definition of these parameters is based on the droplet volume V since we care to identify the deformation of a specific fluid volume V which may be attached to a solid surface in many possible initial configurations and undergo simple shear flow at different flow rates (or Ca).

For the majority of our computations, before the initiation of the steady shear flow, the fluids are at hydrostatic equilibrium under a specific gravitational influence (or Bond number B_d) while the drop forms a constant contact angle $\theta=\theta_0$ (measured from within the drop phase) around a circular contact line. In Sec. III F we also consider the case where initially the fluids may not be at hydrostatic equilibrium for a desired Bond number.

Assuming low-Reynolds-number conditions for both fluid phases, the flow over the drop interface S_d may be described by the boundary integral formula,

$$\begin{aligned}\Omega \boldsymbol{u}(\boldsymbol{x}_0)-\Omega_\infty \boldsymbol{u}^\infty(\boldsymbol{x}_0) &= -\int_{S_2}[\boldsymbol{S}\cdot(\boldsymbol{f}_2-\boldsymbol{f}^\infty)-\mu \boldsymbol{T}\cdot(\boldsymbol{u}_2-\boldsymbol{u}^\infty)\cdot\boldsymbol{n}]\mathrm{d}S \\ &+\int_{S_1}(\boldsymbol{S}\cdot\boldsymbol{f}_1-\lambda\mu\boldsymbol{T}\cdot\boldsymbol{u}_1\cdot\boldsymbol{n})\mathrm{d}S \\ &-\int_{S_d}\{\boldsymbol{S}\cdot(\Delta\boldsymbol{f}-\boldsymbol{f}^\infty)-\mu\boldsymbol{T}\cdot[(1-\lambda)\boldsymbol{u}-\boldsymbol{u}^\infty]\cdot\boldsymbol{n}\}\mathrm{d}S,\end{aligned} \tag{3}$$

where S_1 is the portion of the solid surface wetted by the drop and S_2 is the remaining solid surface.[6] Note that $\boldsymbol{S}$ is the fundamental solution for the three-dimensional Stokes equations and $\boldsymbol{T}$ is the associated stress, while $\boldsymbol{n}$ is the unit normal which we choose to point into fluid 2. The coefficient Ω takes values $4\pi\mu(1+\lambda)$, $4\pi\lambda\mu$, and $4\pi\mu$ for points $\boldsymbol{x}_0$ on the surfaces S_d, S_1, and S_2, respectively, while Ω_∞ takes the value $4\pi\mu$ for points $\boldsymbol{x}_0$ on the surfaces S_d and S_2, and zero for points on the surface S_1.

It is of interest to note that the requirement for low-Reynolds number in the interior flow is not formally valid for very small viscosity ratios. For low-viscosity/inviscid droplets ($\lambda \ll 1$), our computations require that the inner shear stress and pressure change are very small compared to the exterior stresses. As discussed by Dimitrakopoulos and Higdon,[17] for $\lambda \ll 1$ this condition remains valid for arbitrary interior Reynolds number, as long as the exterior Reynolds number is very small. (See the Appendix in Ref. 17.)

At the interface, the boundary conditions on the velocity $\boldsymbol{u}$ and surface stress $\boldsymbol{f}$ are

$$\boldsymbol{u}_1 = \boldsymbol{u}_2 = \boldsymbol{u}, \tag{4}$$

$$\Delta \boldsymbol{f} = \boldsymbol{f}_2 - \boldsymbol{f}_1 = \gamma(\nabla \cdot \boldsymbol{n})\boldsymbol{n} + (\rho_2 - \rho_1)(\boldsymbol{g} \cdot \boldsymbol{x})\boldsymbol{n}, \tag{5}$$

where the subscripts designate quantities evaluated in fluids 1 and 2, respectively.

The interfacial shape $\boldsymbol{x}$ evolves over time based on the kinematic condition at the interface,

$$\frac{d\boldsymbol{x}}{dt} = (\boldsymbol{u} \cdot \boldsymbol{n})\boldsymbol{n}. \tag{6}$$

In order to determine the droplet shape as a function of time, we employ our fully implicit spectral boundary element algorithm for interfacial dynamics in Stokes flow.[21] Our method is based on a mathematically rigorous combination of implicit schemes with our Jacobian-free three-dimensional Newton method,[6] and thus it has strong stability properties which permit the utilization of large time steps, independent of the space discretization. In essence, our implicit interfacial algorithm removes the penalty of a large number of time steps required to monitor the deformation of the fluid interface associated with the commonly employed explicit time-integration interfacial methodologies. For the efficient determination of the equilibrium deformation in a wide range of subcritical flow rates, we utilize our Newton method for equilibrium interfaces under flow conditions.[6]

The numerical solution of our algorithms is achieved through an extension of the spectral boundary element method,[6,22] and thus our methodologies achieve exponential convergence in the numerical accuracy of determining the interfacial shape, without being affected by the disadvantage of the spectral methods for partial differential equations to create denser systems. The interested reader is referred to our relevant papers for more details on the fully implicit and the Newton interfacial methods.[6,21]

The adherent droplets are described by employing a discretization of $N_E=24$ (quadrilateral) spectral elements. The surface of the drop is projected onto a cube whose faces are subdivided into a total of 11 elements as shown in Figs. 3(c) and 4(c) below. The wetted area S_1 on the solid surface is discretized into five elements while the outer solid surface S_2 is discretized into two rows of four elements each. In our computations, the outer solid surface (which formally should extend to infinity) covers an area of at least 10 times the radius of the contact line which is sufficient to produce negligible error in all cases.

Our computational results presented in Secs. III A–III E were derived by employing $N_B=7-9$ basis points along each curvilinear direction of the spectral elements. In our fully implicit algorithm we utilize the third-order diagonally implicit Runge-Kutta scheme. For low and moderate viscosity ratio, $\lambda \leq 1$, we mainly employed a time step $\Delta t=0.1$; for droplets with high viscosity ratio, $\lambda=10$, a time step $\Delta t=1$ was used. For our results presented in Sec. III F, which show large variations in short time periods and the contact line tends rapidly to be tangential to the solid surface, we employed smaller time steps (i.e., $\Delta t=0.02, 0.01$) and $N_B=8-10$ basis points so that we have sufficient space discretization for accurate solution. In Sec. III F we also employed a multiple time-step approach as described in the caption of Figs. 17 and 19, shown below. The accuracy of our results was verified by employing smaller time steps and different basis points for several representative cases; these comparisons show that our results are accurate to at least three significant digits, and thus if we include them on the same plot, they show no difference. The three-dimensional droplet shapes presented here were derived from the actual spectral grid by spectrally interpolating to $N_B=20$.

The present problem depends on the Bond number B_d, the capillary number Ca, the viscosity ratio λ, and the initial angle θ_0. Since our results for different low and moderate flow rates Ca show similar behavior, we restrict our presentation to Ca=0.10 so that we are able to identify the influence of the rest parameters. An exception is Sec. III E where we collect our results on the equilibrium deformation of viscous and inviscid droplets for a wide range of low and moderate (subcritical) flow rates.

III. RESULTS

A. Quiescent drop shape under gravity

The first step in our computations was to determine the (axisymmetric) droplet shape for a given initial angle θ_0 (with $\theta_R \leq \theta_0 \leq \theta_A$) and Bond number $B_d \neq 0$ under quiescent conditions, i.e., Ca=0. This physical system may represent a droplet which has been attached on a solid surface under quiescent conditions, formed a (stationary) circular contact line, and acquired its hydrostatic shape for a given Bond number without violating the hysteresis condition, Eq. (1). To achieve this, we employed our Newton method for equilibrium interfaces under Stokes flow conditions.[6] The initial shape was that of a spherical cap with the desired initial angle θ_0, and by specifying Ca=0 we let our Newton method determine the quiescent shape under different positive and negative Bond numbers by seeking the optimal contact line shape under these conditions (as described in Sec. 2.3 of our earlier study).

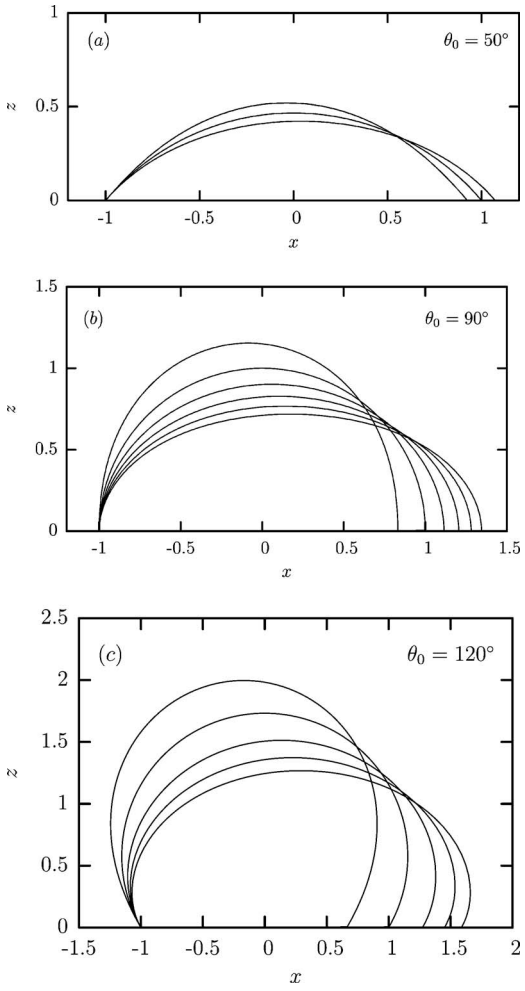

FIG. 1. Profiles of an adherent droplet under quiescent conditions for (a) $\theta_0=50°$ and $B_d=-0.5,0,0.5$; (b) $\theta_0=90°$ and $B_d=-0.5,0,0.5,1,1.5,2$; (c) $\theta_0=120°$ and $B_d=-0.3,0,0.5,1,1.5$.

Figure 1 shows the quiescent droplet profile (i.e., theintersection of droplet surface with the plane $y=0$) for $\theta_0=50°$, 90°, 120° and several Bond numbers. As expected, a negative Bond number results in an upward-extended droplet with larger height and smaller length/width compared to those for $B_d=0$. The opposite happens for positive Bond numbers where the flattened drops show a larger wetted area.

Beyond the obvious changes on the drop's height and width, the Bond number also affects the surface area S_d of the quiescent shape in a more complicated way as shown in Fig. 2. In particular, for $\theta_0=90°$ the spherical cap corresponding to $B_d=0$ shows the minimum surface area S_d as expected. For smaller initial angles, S_d increases monotonically with the Bond number while the opposite happens for larger initial angles. We note that the variation in the droplet's dimensions and surface area with the Bond number provides information on the forces acting on the interface as we discuss later.

B. Droplets with $\theta_0=90°$ and $\lambda=1$

We begin our investigation by considering the effects of Bond number on the deformation of adherent droplets with $\lambda=1$ and $\theta_0=90°$. Figures 3 and 4 show the transient evolution of an adherent droplet for a negative ($B_d=-0.5$) and a positive ($B_d=2$) Bond number, respectively. In both cases, in the upstream portion of the interface, the contact angle is reduced monotonically with time until equilibrium is reached while the opposite happens in the downstream portion.

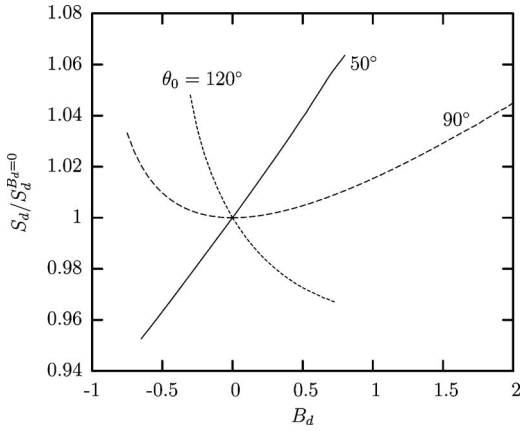

FIG. 2. Variation of the drop surface S_d (scaled with its value for $B_d=0$) with the Bond number, under quiescent conditions for $\theta_0=50°,90°,120°$.

These figures show that the time evolution of the interfacial shape and its properties is similar for both negative and positive Bond numbers, i.e., for both upward-extended and flatter droplets. Figures 3(b) and 4(b) show that the contact angle increases monotonically with the azimuthal angle ϕ from the upstream towards the downstream area of the contact line at all times. Thus, as commonly happens for circular contact lines, the smallest contact angle θ_u at $\phi=180°$ and the largest one θ_d at $\phi=0°$ can be used as a measurement of the interfacial deformation and to provide information on the onset of interfacial sliding (e.g., see Ref. 7).

Figure 5(a) shows the time evolution of the upstream and downstream contact angles, θ_u and θ_d, for an adherent droplet with $\lambda=1$ and $\theta_0=90°$ in simple shear flow with Ca=0.10, and for several Bond numbers (i.e., $B_d=-0.5,0,0.5,1,1.5,2$). This figure clearly reveals that Ca=0.10 is a subcritical flow rate for all these Bond numbers; after the initial transient evolution both angles reach equilibrium where the interfacial shape does not change with time. The contact angles show initially the same evolution for all Bond numbers; however later the droplet with the largest Bond number shows the smaller variation for both upstream and downstream contact angles, θ_u and θ_d, i.e., less deformation. This is also evident in Fig. 5(b) where we plot the time evolution of the contact angle difference $\theta_d-\theta_u$. The droplet profiles at equilibrium for the different Bond numbers are shown in Fig. 5(c).

Therefore, as the Bond number increases, the flatter viscous droplet is more stable for a given flow rate. Equivalently, for specific advancing and receding contact angles, θ_A and θ_R, the flatter droplet requires a higher flow rate to start sliding on the solid surface.

The explanation for the monotonic decrease in deformation as the Bond number increases becomes clear when one considers the forces acting on the droplet. For viscous drop-

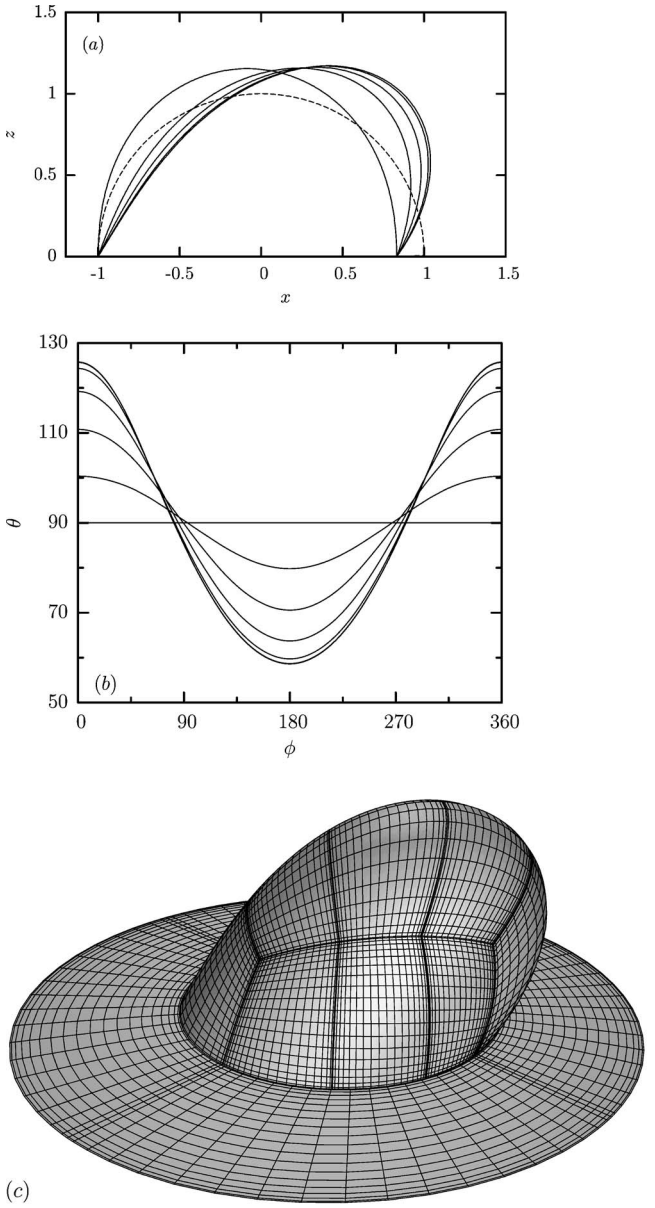

FIG. 3. Deformation of an adherent droplet with $\lambda=1$ and $\theta_0=90°$ in simple shear flow with Ca=0.10 and for $B_d=-0.5$. (a) Droplet profile at times $t=0,0.5,1,2,10$; also included is the undisturbed droplet profile (- -) for $B_d=0$. (b) The variation of the contact angle θ as a function of the azimuthal angle ϕ for times $t=0,0.2,0.5,1,2,4,10$. (The azimuthal angle ϕ is measured with respect to the positive x-direction as usual.) (c) Droplet shape at $t=10$, i.e., at equilibrium.

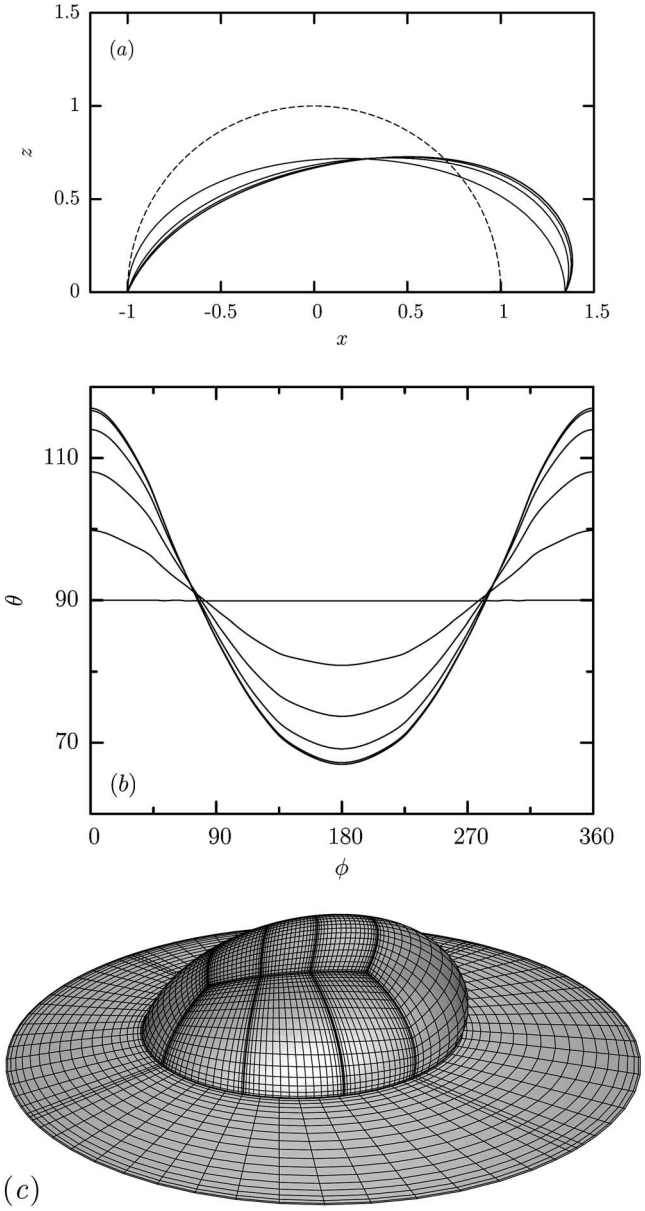

FIG. 4. Deformation of an adherent droplet with $\lambda=1$ and $\theta_0=90°$ in simple shear flow with Ca=0.10 and for $B_d=2$. (a) Droplet profile at times $t=0,0.5,1,2,10$; also included is the undisturbed droplet profile (- -) for $B_d=0$. (b) The variation of the contact angle θ as a function of the azimuthal angle ϕ for times $t=0,0.2,0.5,1,2,4,10$. (c) Droplet shape at $t=10$, i.e., at equilibrium.

lets the dominant deforming force is the shear component F_s of the hydrodynamic force on the interface; F_s is proportional to the shear stress on the drop τ_d and the drop's surface area S_d, i.e., $F_s \sim \tau_d S_d$. Trying to balance this deforming force is the component of surface tension force in the plane of the wall parallel to the flow direction; this restoring force is proportional to the width (or radius) w of the contact region and, for small angle difference $\theta_d - \theta_u$, it scales as

$$F_\gamma \sim (\cos\theta_u - \cos\theta_d)\gamma w. \tag{7}$$

As the Bond number increases, the droplet becomes flatter; the increased width w of the contact region results in an increase for the surface tension force F_γ and thus a smaller deformation.

Our study also provides information on the portions of the contact line which will slide first. To show this, in Fig. 6 we plot the evolution of the contact angle upstream and downstream change, $\theta_0 - \theta_u$ and $\theta_d - \theta_0$, for a negative and a positive Bond number. From this figure it is evident that for small enough hysteresis, during the transient evolution the drops show an early period where both upstream and downstream sliding are equally favorable. During this regime, if the droplet is placed on the solid forming an initial angle $\theta_0 > (\theta_R + \theta_A)/2$, then after some time the downstream por-

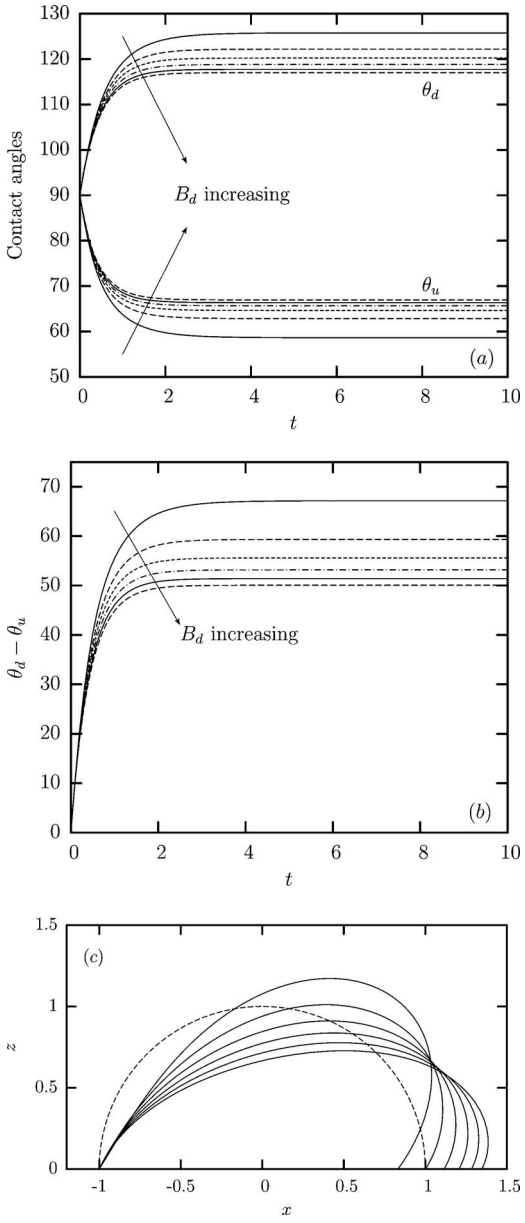

FIG. 5. Deformation of an adherent droplet with $\lambda=1$ and $\theta_0=90°$ in simple shear flow with Ca=0.10 for $B_d=-0.5, 0, 0.5, 1, 1.5, 2$. (a) Time evolution of the upstream and downstream contact angles, θ_u and θ_d. (b) Time evolution of the contact angle difference $\theta_d-\theta_u$. (c) Droplet profile at time $t=10$ (i.e., well past equilibrium); also included is the undisturbed droplet profile (- -) for $B_d=0$.

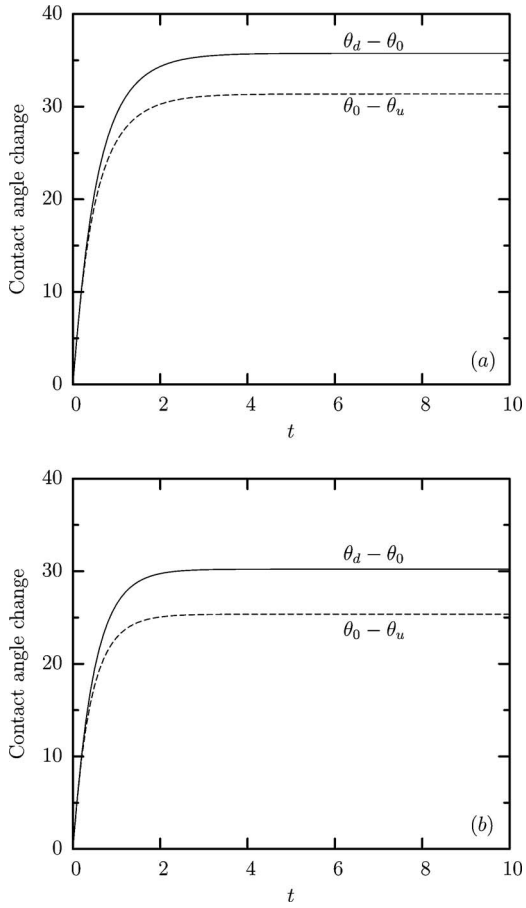

FIG. 6. Time evolution of the contact angle upstream and downstream change, $\theta_0-\theta_u$ and $\theta_d-\theta_0$, for an adherent droplet with $\lambda=1$ and $\theta_0=90°$ in simple shear flow with Ca=0.10. (a) $B_d=-0.5$; (b) $B_d=0.5$.

tion of the drop will slide first. The opposite will happen if the initial angle is $\theta_0<(\theta_R+\theta_A)/2$ where the upstream drop portion will begin moving on the solid substrate. For large enough hysteresis, drops with moderate initial angles θ_0 show a late downstream-favored regime, where the downstream sliding occurs for initial angles $\theta_0>\theta_0^*$ with $\theta_0^*<(\theta_R+\theta_A)/2$.

Thus, with respect to the onset of interfacial sliding, droplets with negative or positive Bond numbers and for moderate initial angles (e.g., $\theta_0=90°$) show similar behavior with those for $B_d=0$ presented in our earlier publication.[7]

C. Influence of the initial angle

We investigate now the gravitational effects on droplets with smaller and larger initial angles. Our computational results for adherent droplets with $\theta_0=50°$ reveal that the deformation of droplets with small contact angles is affected differently by the Bond number compared to those with moderate angles. As shown in Fig. 7, instead of a (clear) monotonic decrease in deformation as the Bond number increases, a droplet with $\theta_0=50°$ is not affected much by the Bond number.

The force balance on these droplets may provide insight on their deformation behavior. Similar to our earlier discussion for $\theta_0=90°$, as the Bond number increases the flatter droplet is accompanied with an increased width w of the contact region which results in an increase for the surface tension force F_γ. However, for small contact angles, as the Bond number increases, the flatter droplet is accompanied with an increase in the surface area S_d and thus an increased shear force F_s. Thus these two opposite actions (i.e., increase in w and S_d) counterbalance the effects of Bond number variation.

We now turn our attention to viscous droplets with large initial angles. Figure 8 shows that for a droplet with $\theta_0=120°$, by increasing the Bond number, the flatter drop shows less deformation, in qualitative agreement with our

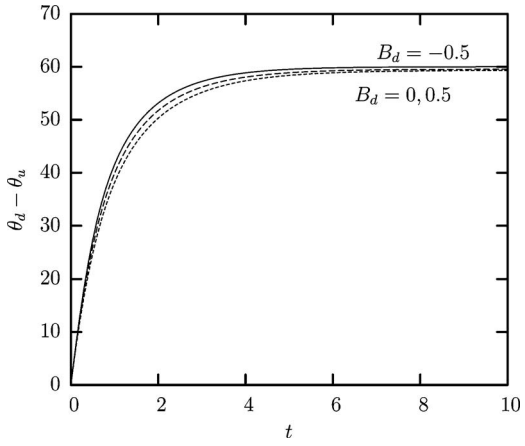

FIG. 7. Time evolution of the contact angle difference $\theta_d - \theta_u$ for an adherent droplet with $\lambda = 1$ and $\theta_0 = 50°$ in simple shear flow with Ca=0.10 and for $B_d = -0.5, 0, 0.5$.

results for $\theta_0 = 90°$ presented earlier in Fig. 5. This figure also reveals that the negative Bond number $B_d = -0.3$ is accompanied with a significant deformation especially at the upstream portion of the droplet. These conclusions are also evident from the deformed droplet profiles presented in Fig. 8(c), where it is shown that for droplets with large initial angles, the downstream portion of the interface tends to become tangential to the solid wall.

The monotonic decrease in deformation as the Bond number increases can be explained based on the interfacial force balance. Similar to our earlier discussion for small and moderate contact angles, as the Bond number increases the flatter droplet is accompanied with an increased surface tension force F_γ due to the increased width w of the contact region. For droplets with large contact angles, as the Bond number increases the flatter droplet is accompanied with a decrease in the surface area S_d and thus a decreased shear force F_s. Both actions (increase in w and decrease in S_d) contribute to the monotonic decrease in deformation as the Bond number increases for droplets with large contact angles. They also justify the larger effects of the Bond number variation on the droplet deformation shown in Fig. 8 with respect to those for droplets with moderate angles presented in Fig. 5.

With respect to the onset of interfacial sliding, our earlier study for $B_d = 0$ (Ref. 7) revealed that droplets with large initial angles $\theta_0 \geq 120°$, after a rather small early equally favorable period, show a large period where downstream sliding is more favorable than the upstream sliding, i.e., downstream sliding occurs for initial angles $\theta_0 > \theta_0^*$ with $\theta_0^* < (\theta_R + \theta_A)/2$. Our present results depicted in Fig. 9 reveal that the gravitational effects on the onset of interfacial sliding for droplets with large initial angles is more complicated.

In particular, this figure demonstrates that a negative Bond number reinforces the behavior found for $B_d = 0$, i.e., an upward-extended droplet shows a much larger upstream change in the contact angle $\theta_0 - \theta_u$ than a downstream change $\theta_d - \theta_0$; thus for such drops downstream sliding is much more favorable than upstream sliding. However, a positive Bond number for droplets with large initial angles θ_0 reverts to the

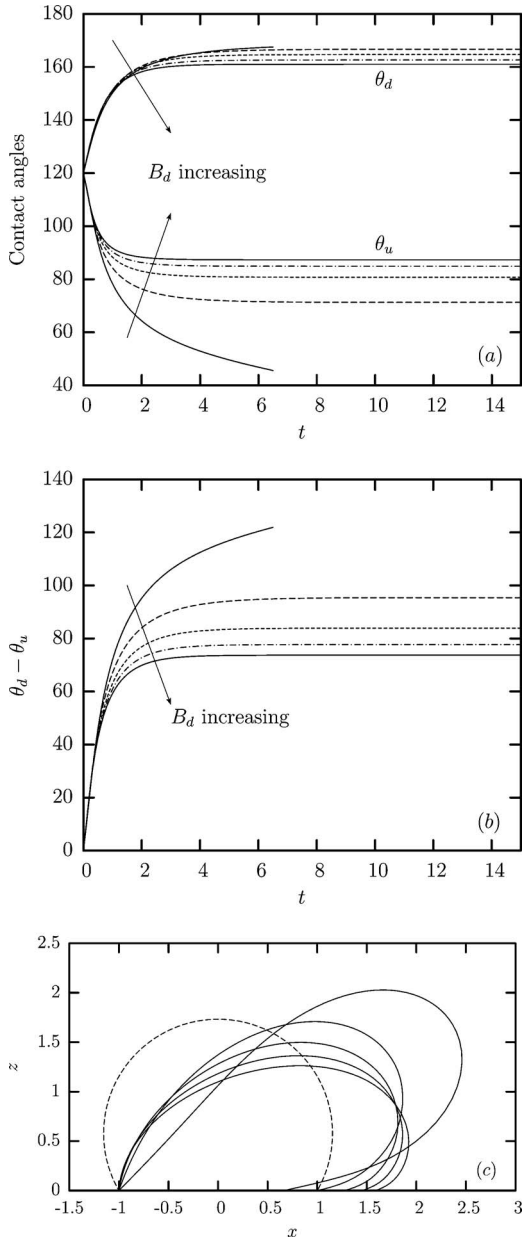

FIG. 8. Deformation of an adherent droplet with $\lambda = 1$ and $\theta_0 = 120°$ in simple shear flow with Ca=0.10, for $B_d = -0.3, 0, 0.5, 1, 1.5$. (a) Time evolution of the upstream and downstream contact angles, θ_u and θ_d. (b) Time evolution of the contact angle difference $\theta_d - \theta_u$. (c) Droplet profile at time $t = 15$ (i.e., well past equilibrium) for $B_d = 0, 0.5, 1, 1.5$, and at time $t = 6.5$ for $B_d = -0.3$; also included is the undisturbed droplet profile (- -) for $B_d = 0$.

behavior of $B_d = 0$. As our results for $B_d = 1.5$ presented in Fig. 9 indicate, the flatter droplet is more prone to slide at its upstream portion.

D. Influence of the viscosity ratio

In this section, we focus our attention on the effects of the viscosity ratio on the deformation of adherent droplets with positive or negative Bond numbers. As discussed earlier, the Bond number affects viscous droplets with small contact angles in a different way than those for moderate and large angles owing to the different variation of the drop surface S_d (and thus the shear force F_s on the drop) with the Bond number.

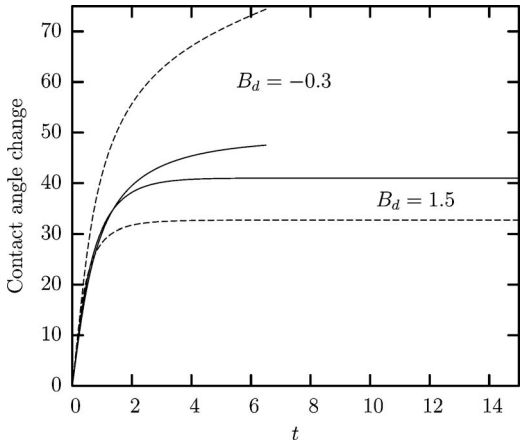

FIG. 9. Deformation of an adherent droplet with $\lambda=1$ and $\theta_0=120°$ in simple shear flow with Ca=0.10. Time evolution of the contact angle downstream and upstream change: (——), $\theta_d-\theta_0$; (- -), $\theta_0-\theta_u$ for $B_d=-0.3,1.5$.

On the other hand, inviscid droplets/bubbles (i.e., $\lambda=0$) exhibit similar behavior with the Bond number, independent of the contact angle, as illustrated in Fig. 10 where we present the time evolution of the contact angle difference $\theta_d-\theta_u$ for several B_d and for $\theta_0=50°,90°,120°$. In all cases, the droplet deformation is decreased as the Bond number increases, i.e., the flatter drops are more stable for all contact angles studied. In addition, droplets with large initial angles (e.g., $\theta_0=120°$) show significant deformation (especially for small Bond numbers) and require more time to reach equilibrium.

The explanation for the monotonic decrease in deformation as the Bond number increases for all initial contact angles becomes clear when one considers the forces acting on the droplet. For inviscid droplets, the deforming force is the pressure force F_p on the interface which is proportional to the drop's frontal area A_d and the pressure change Δp over the drop

$$F_p \sim A_d \Delta p \sim hw\Delta p, \tag{8}$$

where A_d scales with the height h and the width w of the droplet. Comparing Eqs. (8) and (7), one readily realizes that as the Bond number increases, the increased width w of the droplet results in an increase of both the deforming force F_p and the restoring surface tension force F_γ. Therefore, for inviscid droplets, the monotonic decrease in deformation with the Bond number is mainly caused by the decrease of the droplet's height h which occurs for all contact angles.

High-viscosity droplets show similar deformation with that for $\lambda=1$ droplets presented earlier. However, as the viscosity ratio increases from small values, the increased shear force on the droplet results in higher interfacial deformation, e.g., larger $\theta_d-\theta_u$ difference. This is clearly evident in Fig. 11(a) where we present the evolution of the contact angle difference $\theta_d-\theta_u$ for a negative and a positive Bond number and for viscosity ratio $\lambda=0,1,10$. Observe that in this figure the time is scaled with $1+\lambda$ which reflects the fact that the dynamics of droplets with different viscosity ratio evolve on

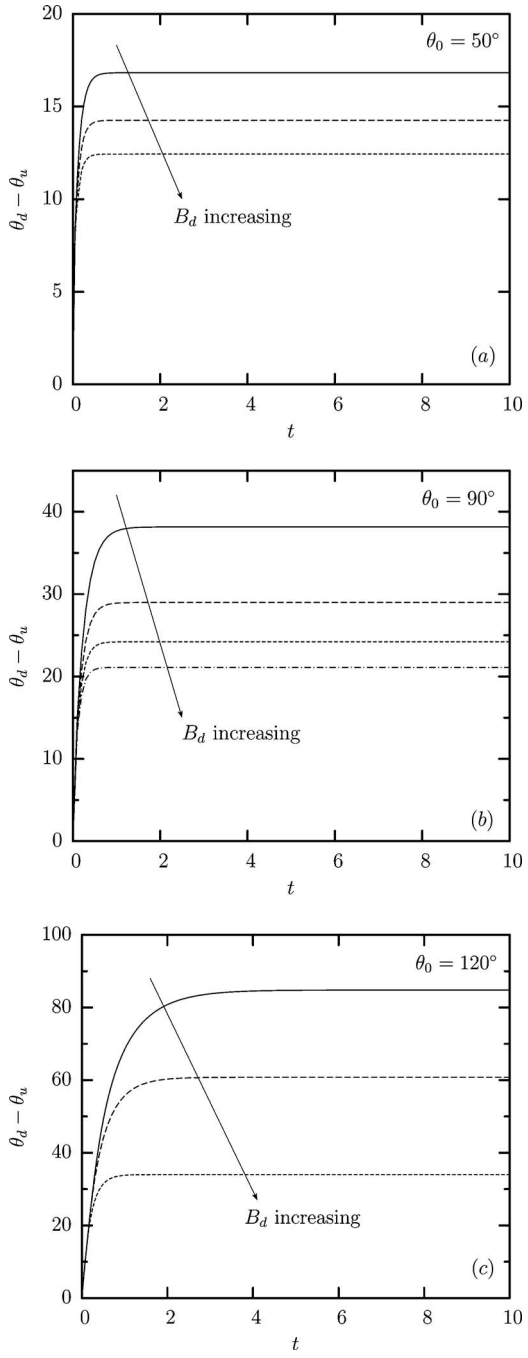

FIG. 10. Deformation of an adherent droplet with $\lambda=0$ in simple shear flow with Ca=0.10. (a) Time evolution of the contact angle difference $\theta_d-\theta_u$ for $\theta_0=50°$ and $B_d=-0.5,0,0.5$. (b) As in (a), but for $\theta_0=90°$ and $B_d=-0.5,0,0.5,1$. (c) As in (a), but for $\theta_0=120°$ and $B_d=-0.3,0,1.5$.

the surface tension time scale which may be described by $\tau_\gamma=(1+\lambda)\mu a/\gamma=(1+\lambda)\mathrm{Ca}\,\tau_f$. The increased interfacial deformation for the high-viscosity droplets is also evident at the equilibrium profiles for droplets with negative and positive Bond numbers as seen in Figs. 11(b) and 11(c). It is of interest to note that, for subcritical flow rates, the droplet deformation reaches an asymptotic (upper) limit for very large viscosity ratios (i.e., $\lambda\to\infty$) as discussed for the case $B_d=0$ by Dimitrakopoulos[7] (see Fig. 7 of the earlier study).

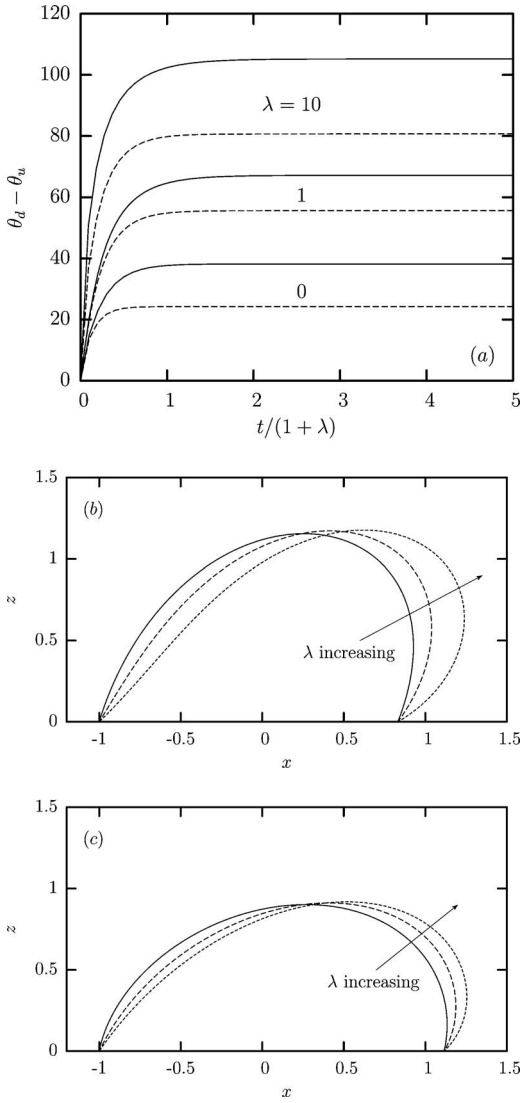

FIG. 11. Influence of the viscosity ratio λ on the deformation of an adherent droplet with θ_0=90° in simple shear flow with Ca=0.10. Viscosity ratios: λ=0,1,10. (a) Time evolution of the contact angle difference $\theta_d - \theta_u$ for Bond number B_d: −0.5 (——) and 0.5 (- -). (b) Droplet profile at equilibrium for B_d=−0.5. (c) As in (b), but for B_d=0.5.

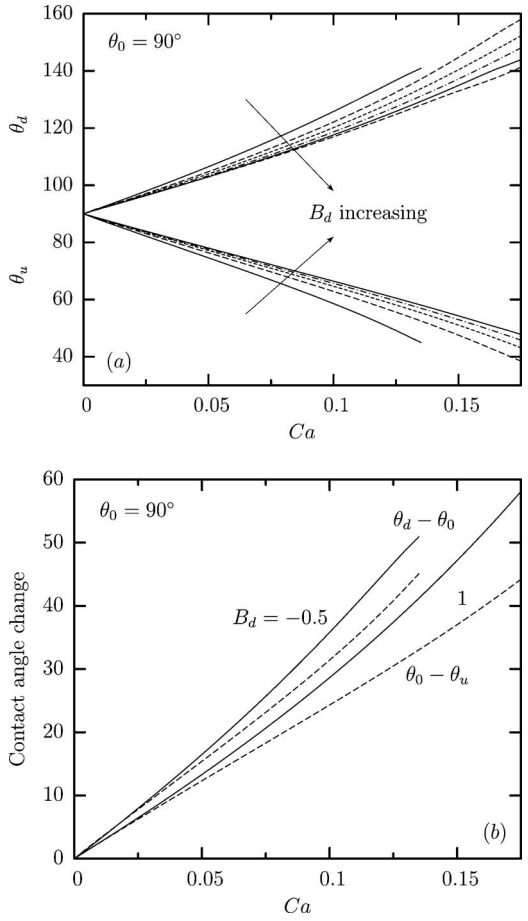

FIG. 12. Equilibrium deformation vs capillary number Ca for an adherent droplet with λ=1 and θ_0=90°. (a) Upstream and downstream contact angles, θ_u and θ_d, for B_d=−0.5,0,0.5,1,1.5,2. (b) Contact angle downstream and upstream change: (——), $\theta_d - \theta_0$; (- -), $\theta_0 - \theta_u$, for B_d=−0.5,1.

E. Equilibrium deformation of adherent droplets

In the previous three subsections we presented the dynamics of the interfacial deformation by considering both the transient evolution and the equilibrium conditions for a representative flow rate (i.e., Ca=0.1). In this section, we consider the equilibrium deformation of attached droplets versus Ca for a wide range of low and moderate (subcritical) flow rates. To derive these equilibrium conditions, we employed our Newton method for equilibrium interfaces under Stokes flow conditions.[6] Our results here verify our earlier conclusions (presented in Secs. III B–III D) while they provide numerical data over a range of low and moderate flow rates.

Figure 12(a) shows the equilibrium variation of the upstream and downstream contact angles, θ_u and θ_d, with the capillary number Ca for an adherent droplet with λ=1 and θ_0=90° and for different Bond numbers. In agreement with our conclusions in Sec. III B, the equilibrium deformation decreases as the Bond number increases owing to the increased surface tension force which accompanies the flatter interfacial shape. In addition, at equilibrium the downstream portion of the drop shows a higher deformation than its upstream portion for both negative and positive Bond numbers as shown in Fig. 12(b).

The influence of the Bond number on the equilibrium variation of the upstream and downstream contact angles for a viscous droplet with θ_0=120° is similar to that for θ_0=90° as shown in Fig. 13(a). As discussed in Sec. III C, for large initial angles θ_0, the monotonic decrease of the interfacial deformation with the Bond number results from both the increased surface tension force and the decreased shear force (which accompanies the decreased surface area). In addition, Fig. 13(b) shows that while negative Bond numbers cause a higher upstream deformation compared to the downstream deformation, this behavior is reverted for positive Bond numbers.

The limited influence of the Bond number on the equilibrium variation of the upstream and downstream contact angles with the capillary number Ca for a viscous droplet with θ_0=50° is shown in Fig. 14. As discussed in Sec. III C,

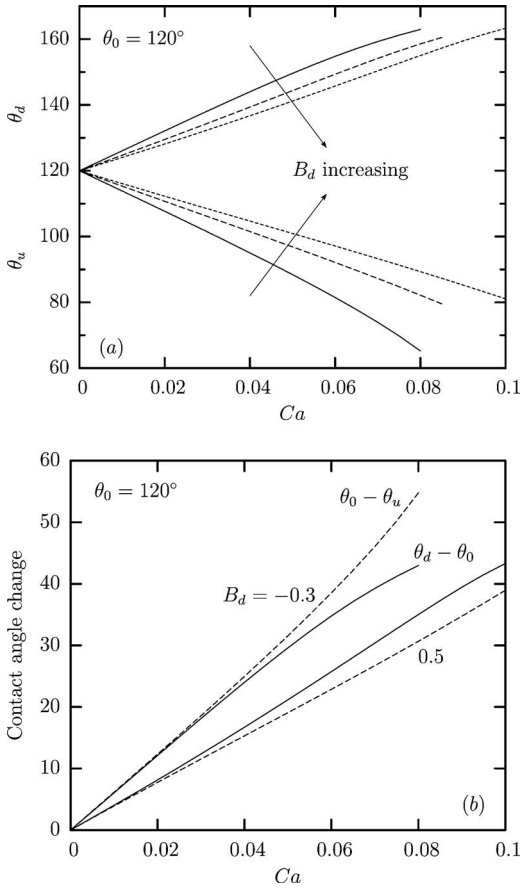

FIG. 13. Equilibrium deformation vs capillary number Ca for an adherent droplet with $\lambda=1$ and $\theta_0=120°$. (a) Upstream and downstream contact angles, θ_u and θ_d, for $B_d=-0.3,0,0.5$. (c) Contact angle downstream and upstream change: (——), $\theta_d-\theta_0$; (- -), $\theta_0-\theta_u$, for $B_d=-0.3,0.5$.

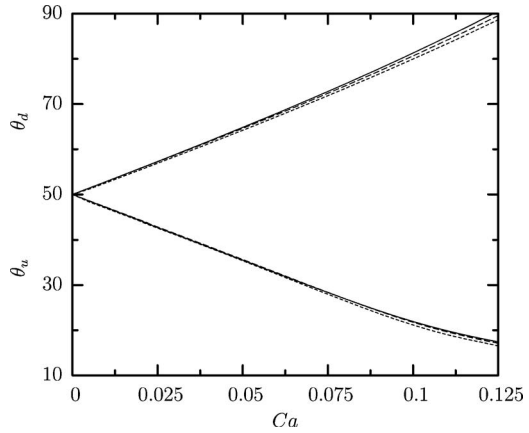

FIG. 14. Variation of the equilibrium upstream and downstream contact angles, θ_u and θ_d, with the capillary number Ca for an adherent droplet with $\lambda=1$ and $\theta_0=50°$. Bond number B_d: (——), −0.5; (– –), 0; (- - - -), 0.5.

this is a consequence of the fact that, for small initial angles θ_0, both the shear force and the surface tension force increase with the Bond number.

As discussed in Sec. III D, inviscid droplets or bubbles show a similar behavior with the Bond number independently of the initial contact angle θ_0 as clearly shown in Fig. 15 over a wide range of flow rates. In this case, the monotonic decrease of the drop's height with the Bond number results in a decrease of the deforming pressure force and thus of the interfacial deformation.

Figure 16 shows the effects of the viscosity ratio λ on the droplet deformation for a negative and a positive Bond number. As the viscosity ratio increases from small values, the increased viscous force causes a higher equilibrium deformation, i.e., a higher variation of the upstream and downstream contact angles.

F. Influence of the initial shape

In the previous sections we have considered attached droplets which, before the initiation of the steady shear flow, are at hydrostatic equilibrium under a specific gravitational influence. However, a droplet may be attached to a solid surface without being at hydrostatic equilibrium (under a desired Bond number) at the instance of the flow initiation. In such a case, the drop may follow a different transient deformation compared to those presented so far.

Figure 17(a) shows the time evolution of the upstream and downstream contact angles, θ_u and θ_d, for an adherent droplet with $\lambda=1$ and $B_d=2$ in simple shear flow with Ca $=0.10$. The initial drop shape is a spherical cap with θ_0 $=90°$. For the same (circular) contact line and for this Bond number, the hydrostatic shape is flatter showing a contact angle $\theta_0\approx116.7°$. The evolution of the downstream contact angles θ_d is similar to that presented earlier, i.e., this angle shows a monotonic increase towards its equilibrium value. On the other hand, the upstream contact angle θ_u shows an evolution which has not been observed so far. Instead of a monotonic decrease, this angle first increases towards a maximum of $\theta_u\approx100.2°$ near $t=0.16$, and then decreases towards its equilibrium value. The nontrivial contact angle evolution in the upstream portion of the contact line is demonstrated in Fig. 17(b), where we present the variation of the contact angle around the contact line for several times.

This contact angle evolution can be understood if we consider that in this case the drop is under the influence of both the shear flow and the gravitational forcing (due to the fact that the initial shape differs from the hydrostatic one). The former tends to decrease the upstream contact angle and increase the downstream angle while the latter tends to make the drop shape flatter. Since for $B_d=2$ the hydrostatic shape shows a contact angle $\approx116.7°$ (i.e., greater than that of the initial shape), the gravitational forcing tends to increase the contact angle all around the contact line. At the downstream portion of the contact line both actions tend to increase the contact angle. On the other hand, at the upstream portion of the contact line the two actions have opposite effects. The maximum in θ_u at the early times reveals that initially the gravitational deformation (due to the fact that the initial shape differs from the hydrostatic one) dominates the flow-induced deformation, and the drop tends towards its hydrostatic shape; the latter is however never completely reached due to the flow-induced deformation. As shown in Fig. 17(a), after the influence of this gravitational forcing has ceased

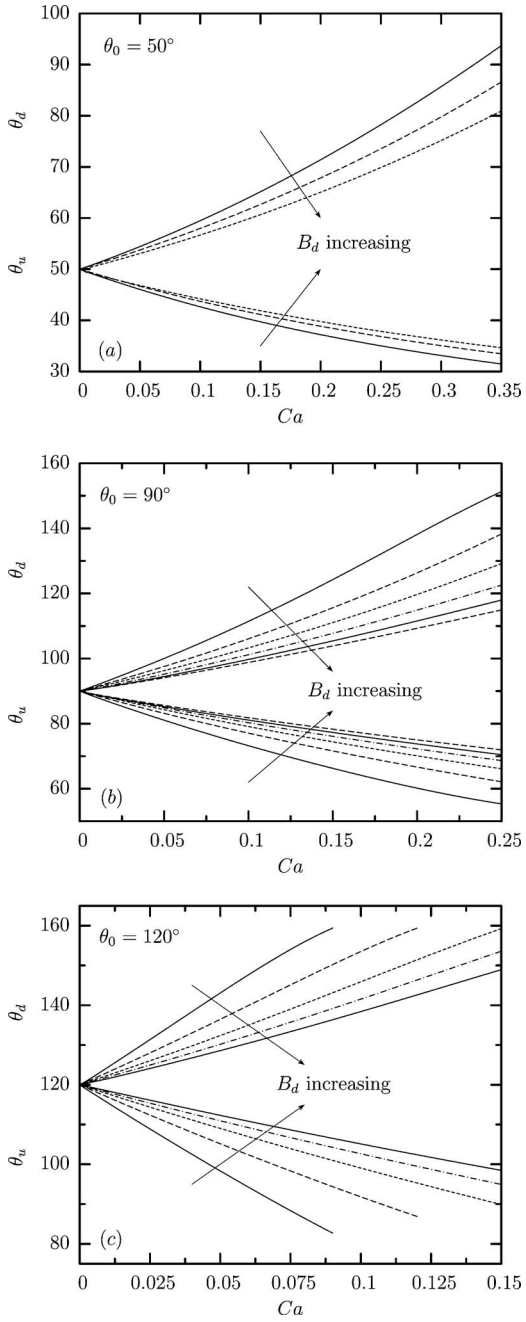

FIG. 15. Upstream and downstream contact angles, θ_u and θ_d vs capillary number Ca for an adherent droplet with $\lambda=0$. (a) $\theta_0=50°$ and $B_d=-0.5,0,0.5$. (b) $\theta_0=90°$ and $B_d=-0.5,0,0.5,1,1.5,2$. (c) $\theta_0=120°$ and $B_d=-0.3,0,0.5,1,1.5$.

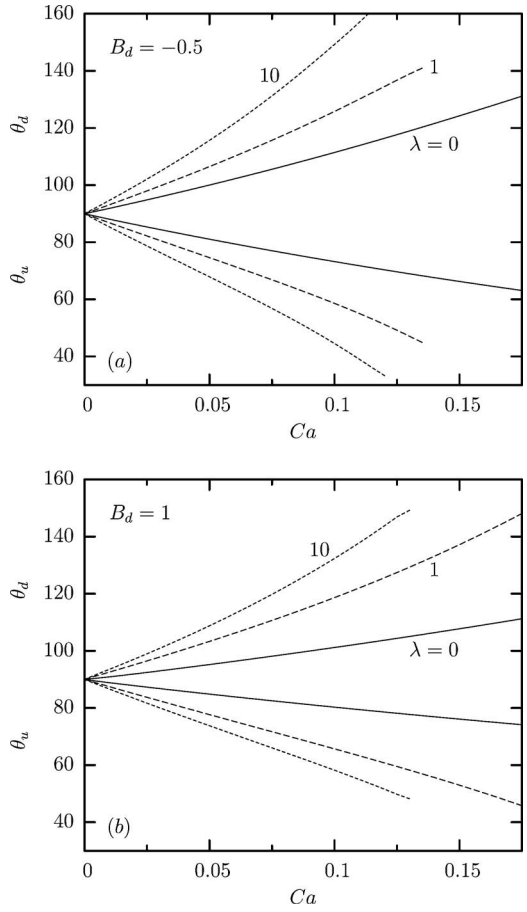

FIG. 16. Upstream and downstream contact angles, θ_u and θ_d vs capillary number Ca for an adherent droplet with $\theta_0=90°$ and for viscosity ratio: $\lambda=0,1,10$. (a) $B_d=-0.5$; (b) $B_d=1$.

(i.e., around $t=1$), the droplet follows the same evolution with that when the initial shape is the hydrostatic one.

The effects of the gravitational forcing on the contact angle evolution are more pronounced when the drop's initial shape differs considerably from its hydrostatic shape. This is depicted in Fig. 18 where we present the deformation of a droplet whose initial shape is a spherical cap under the large Bond number $B_d=4$. It is of interest to note that in this case the combined action of the shear flow and the increased gravitational forcing causes the downstream portion of the droplet to become rapidly tangential to the solid plane, i.e., the downstream contact angle shows a fast increase towards the limit of 180°. We emphasize that, with respect to the onset of interfacial sliding, this type of experiment makes the downstream sliding much more favorable than the upstream sliding.

To investigate the case where the initial drop shape is flatter than its hydrostatic configuration for a specific Bond number, in Fig. 19 we present the time evolution of the upstream and downstream contact angles, θ_u and θ_d, for an adherent droplet with $\lambda=1$ and $B_d=-2$ in simple shear flow with Ca=0.10. The initial drop shape is a spherical cap with $\theta_0=90°$ while for the same (circular) contact line and for this Bond number the hydrostatic shape is more upward-extended showing a contact angle $\theta_0\approx 72.7°$.

In this case, the combined action of the shear flow and the gravitational forcing (due to the fact that the initial shape differs from the hydrostatic one) tend to decrease faster than the contact angle in the upstream portion of the contact line. In the downstream area, the two forces have opposite effects while at early times the gravitational deformation dominates the flow-induced deformation, and θ_d shows a local minimum before its final increase towards its equilibrium value. We emphasize that this gravitational influence is restricted to early times only; afterwards the droplet tends to follow the same evolution with that when the initial shape is the hydro-

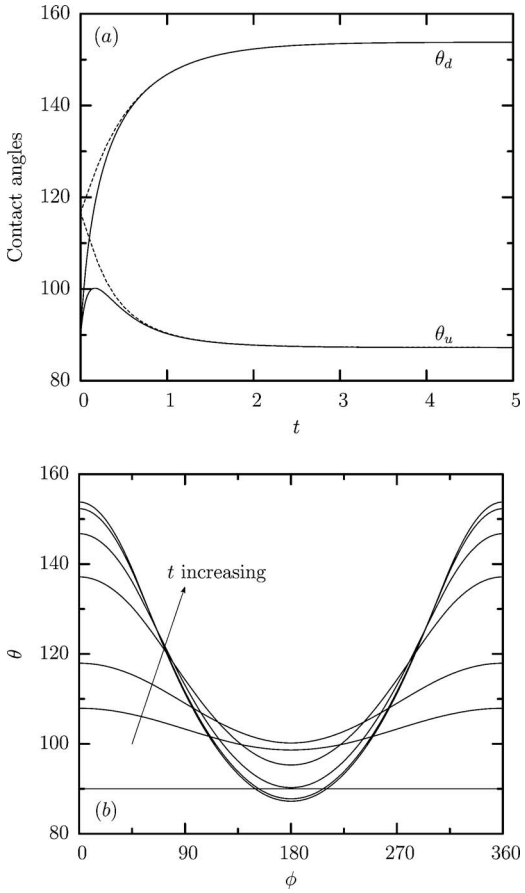

FIG. 17. Deformation of an adherent droplet with $\lambda=1$ and $B_d=2$ in simple shear flow with Ca=0.10; the initial drop shape is a spherical cap with $\theta_0=90°$. (a) Time evolution of the upstream and downstream contact angles, θ_u and θ_d. Also included are the results (- -) when the initial drop shape is the hydrostatic shape which shows $\theta_0=116.7°$. (b) The variation of the contact angle θ as a function of the azimuthal angle ϕ for times $t=0,0.08,0.16,0.5,1,2,10$. A multiple time-step approach was used with $\Delta t=0.02$ for the time period $[0,1]$ and $\Delta t=0.1$ for $[1,10]$.

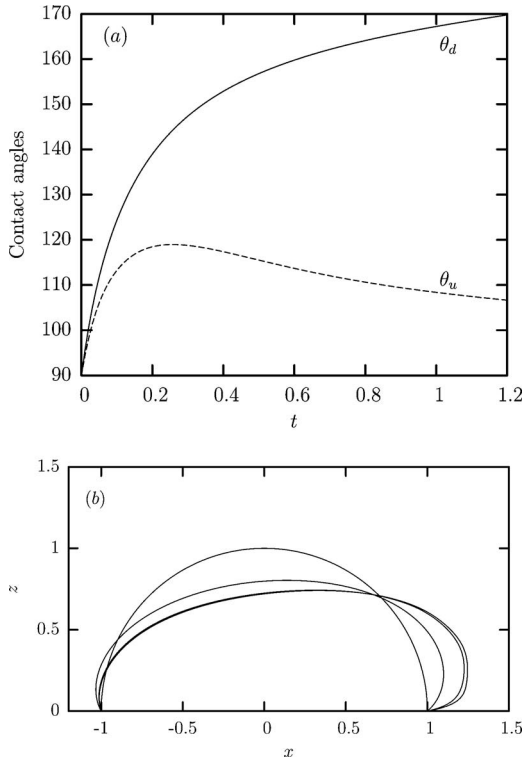

FIG. 18. Deformation of an adherent droplet with $\lambda=1$ and $B_d=4$ in simple shear flow with Ca=0.10; the initial drop shape is a spherical cap with $\theta_0=90°$. (a) Time evolution of the upstream and downstream contact angles, θ_u and θ_d. (b) Droplet profile at times $t=0,0.2,1,1.2$.

IV. DISCUSSION

In this paper we have considered the gravitational effects (i.e., the influence of positive and negative Bond numbers) on the deformation of viscous and inviscid droplets adhering to horizontal rough solid surfaces in steady shear Stokes flows. We have also identified the gravitational effects on the onset of interfacial sliding, i.e., on the portions of the contact line which slide first due to violation of the hysteresis condition. We have considered different initial configurations in-

static one. In addition, this type of experiments makes upstream interfacial sliding much more favorable than downstream sliding.

For the same type of experiments, by reducing further the Bond number, the observed behavior is more pronounced as shown in Figs. 20 and 21 where we present the evolution of a droplet whose initial shape is a spherical cap for $B_d=-2$ and $B_d=-4$, respectively. As shown in Fig. 20 the Bond number $B_d=-2$ causes a very fast decrease of the upstream contact angle and thus the upstream portion of the droplet becomes rapidly tangential to the solid surface. On the other hand, at the downstream portion the flow dominates eventually the gravitational forcing and thus after the early minimum, the downstream contact angle increases. By reducing further the Bond number to $B_d=-4$ seen in Fig. 21, the increased negative gravitational forcing causes a very fast upward motion of the entire droplet and thus both the upstream and downstream portion of the droplet tend now to become tangential to the solid surface.

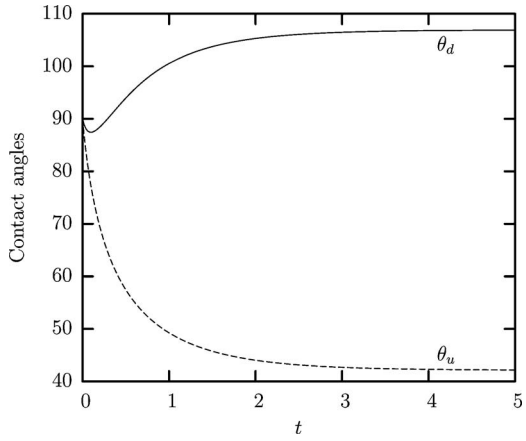

FIG. 19. Time evolution of the upstream and downstream contact angles, θ_u and θ_d, for an adherent droplet with $\lambda=1$ and $B_d=-1$ in simple shear flow with Ca=0.10; the initial drop shape is a spherical cap with $\theta_0=90°$. A multiple time-step approach was used with $\Delta t=0.02$ for the time period $[0,2]$ and $\Delta t=0.1$ for $[2,10]$.

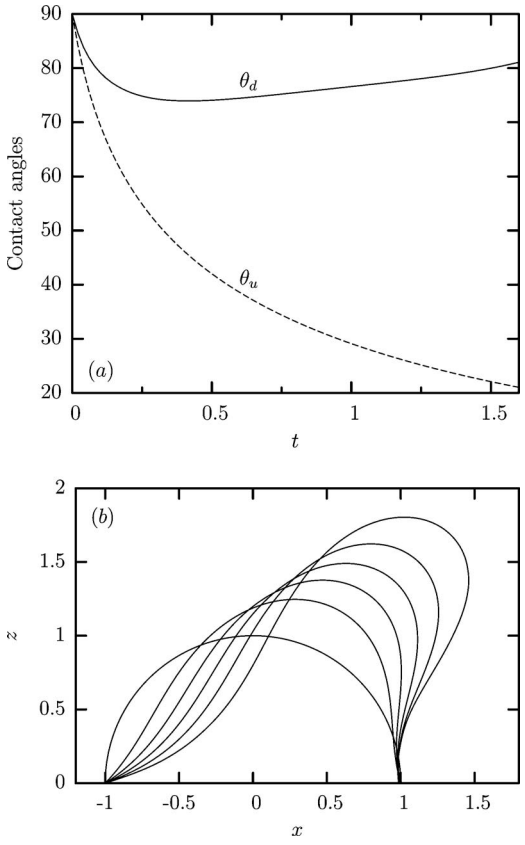

FIG. 20. Deformation of an adherent droplet with $\lambda=1$ and $B_d=-2$ in simple shear flow with Ca=0.10; the initial drop shape is a spherical cap with $\theta_0=90°$. (a) Time evolution of the upstream and downstream contact angles, θ_u and θ_d. (b) Droplet profile at times $t=0,0.4,0.8,1.2,1.6,2$.

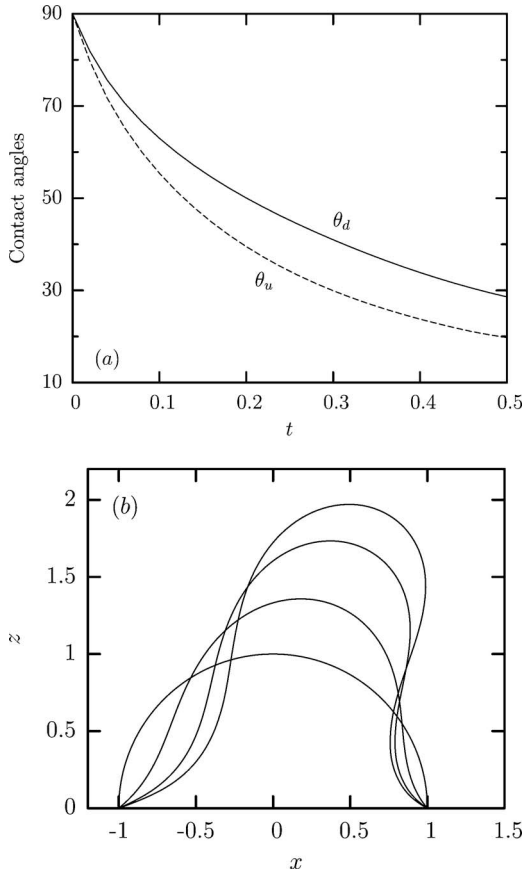

FIG. 21. Deformation of an adherent droplet with $\lambda=1$ and $B_d=-4$ in simple shear flow with Ca=0.10; the initial drop shape is a spherical cap with $\theta_0=90°$. (a) Time evolution of the upstream and downstream contact angles, θ_u and θ_d. (b) Droplet profile at times $t=0,0.2,0.4,0.5$.

cluding drops which are at hydrostatic equilibrium for the desired Bond number at the instance of the flow initiation as well as fluids which are not at hydrostatic equilibrium.

When the interfacial system is at hydrostatic equilibrium at the initiation of a steady shear flow, our study shows that the Bond number affects the deformation of viscous droplets with moderate and large initial contact angles in a different way than those for small angles. In particular, the former shows a monotonic decrease in deformation as the Bond number increases as a result of the associated increase of the drop's width and thus the restoring surface tension force for the flatter, high Bond number, droplets. This behavior is more pronounced for droplets with large initial contact angles which are also accompanied with a decrease in their surface area and thus in the deforming shear force. On the other hand for small contact angles, as the Bond number increases, the flatter viscous droplet is accompanied with an increased shear force (owing to the increase of the drop's surface area) as well as with an increase in the surface tension force. These opposite actions counterbalance the effects of Bond number increase and thus the deformation of droplets with small contact angles is not affected much by the Bond number.

Inviscid droplets with different initial contact angles show similar behavior as the Bond number increases, i.e., their deformation is monotonically decreased. In this case, the increase of the drop width for the flatter, high Bond number droplets results in an increase in the restoring surface tension force but also in the deforming force (which for inviscid droplets/bubbles is the pressure force). Therefore, for inviscid droplets, the monotonic decrease in deformation with the Bond number is mainly caused by the decrease of the droplet's height which occurs for all contact angles.

We emphasize that our forces' analysis, which helps to explain our numerical results of the gravitational influence on the drop deformation, relies mostly on the effects of the Bond number on the drop geometric characteristics, i.e., its width, height, and surface area. However, the deforming shear and pressure forces are also affected by physical variables, i.e., the shear stress on the drop τ_d and the pressure change Δp over the drop, respectively. These physical variables are (implicit) functions of the drop shape and are not expected to change our aforementioned analysis. This is supported by the scaling analysis for small angles which predicts that $\tau_d \sim \mu G$ and $\Delta p \sim \theta_0 \mu G$, i.e., they are not affected by the Bond number.

With respect to the onset of interfacial sliding, our study shows that droplets under positive or negative Bond numbers show similar behavior to that for $B_d=0$ identified in our earlier work.[7] In particular, droplets with small and moderate initial angles show an early period where both upstream and downstream sliding are equally favorable as well as a late downstream-favored period; by contrast, droplets with large

initial angles, after a rather small early equally favorable period, show a large period where downstream sliding is more favorable than the upstream sliding. In addition, for droplets with large initial angles our present study shows that a negative Bond number reinforces the behavior found for $B_d=0$, i.e., upward-extended droplets exhibit a more favorable downstream initial sliding. For the same case, positive Bond numbers weaken this behavior while large enough Bond numbers revert to the behavior of $B_d=0$, i.e., they make upstream sliding more favorable.

When the interfacial system is not at hydrostatic equilibrium at the initiation of a steady shear flow, its dynamic evolution is more complicated. In this case the droplet deformation is affected by both the shear flow and the gravitational forcing (due to the fact that the initial shape differs from the hydrostatic one). When the drop is initially more upward-extended than its hydrostatic shape, both forces contribute to a fast increase of the downstream contact angle; however at the upstream portion of the contact line they have opposite effects. As a result at early times the gravitational deformation dominates the flow-induced deformation and initially the upstream contact angle increases towards a local maximum before its final flow-induced decrease. For large deviations from the hydrostatic shape, the increased gravitational forcing causes the downstream portion of the droplet to rapidly become tangential to the solid surface. Thus, this case makes the downstream sliding much more favorable than the upstream sliding. The opposite happens for droplets which are initially flatter than their hydrostatic configurations. Therefore this type of experiments can be employed to initiate interfacial sliding at a desired portion of the contact line.

As discussed in Sec. I above, earlier studies have commonly ignored the gravitational effects on the drop deformation. One exception is the work by Dimitrakopoulos and Higdon[5] who considered the equilibrium conditions just before the (final) flow-induced drop displacement from rigid boundaries for zero and positive Bond numbers. Via computational work and asymptotic analysis based on small-angle lubrication theory, Dimitrakopoulos and Higdon[5] demonstrated that for a given flow rate, the deformation of viscous two-dimensional droplets is increased with the Bond number due to the corresponding increase of the drop's length. They also showed that the opposite happens for two-dimensional inviscid droplets due to the decrease of the drop height.

Therefore, the present study has shown that the gravitational influence on a three-dimensional droplet differs considerably for that on a two-dimensional drop (i.e., a cylindrical cap) owing to the ability of the three-dimensional droplets to expand or contract in the lateral (i.e., cross-flow) direction changing the interfacial dynamics. In essence, our present work identifies the three-dimensional nature of the deformation and sliding of adherent droplets which has also been demonstrated in the earlier work of Dimitrakopoulos and Higdon on the yield criteria for displacement of three-dimensional droplets,[6,16–18] and the recent experiments of Podgorski *et al.*[23]

ACKNOWLEDGMENTS

This work was supported in part by the National Science Foundation. Acknowledgment is made to the Donors of the American Chemical Society Petroleum Research Fund for partial support of this research. Some computations were performed on multiprocessor supercomputers provided by the National Center for Supercomputing Applications (NCSA) in Illinois.

[1] J. Bear, *Dynamics of Fluids in Porous Media* (Dover, New York, 1972).
[2] H. A. Stone, A. D. Stroock, and A. Ajdari, "Engineering flows in small devices: Microfluidics toward a lab-on-a-chip," Annu. Rev. Fluid Mech. **36**, 381 (2004).
[3] V. Cristini and Y.-C. Tan, "Theory and numerical simulation of droplet dynamics in complex flows: A review," Lab Chip **4**, 257 (2004).
[4] R. O. Hynes, "Integrins, versatility, modulation and signaling in cell adhesion," Cell **69**, 11 (1992).
[5] P. Dimitrakopoulos and J. J. L. Higdon, "Displacement of fluid droplets from solid surfaces in low-Reynolds-number shear flows," J. Fluid Mech. **336**, 351 (1997).
[6] P. Dimitrakopoulos and J. J. L. Higdon, "On the displacement of three-dimensional fluid droplets from solid surfaces in low-Reynolds-number shear flows," J. Fluid Mech. **377**, 189 (1998).
[7] P. Dimitrakopoulos, "Deformation of a droplet adhering to a solid surface in shear flow: Onset of interfacial sliding," J. Fluid Mech. **580**, 451 (2007).
[8] J. Q. Feng and O. A. Basaran, "Shear flow over a translationally symmetric cylindrical bubble pinned on a slot in a plane wall," J. Fluid Mech. **275**, 351 (1994).
[9] X. Li and C. Pozrikidis, "Shear flow over a liquid drop adhering to a solid surface," J. Fluid Mech. **307**, 167 (1996).
[10] A. D. Schleizer and R. T. Bonnecaze, "Displacement of a two-dimensional immiscible droplet adhering to a wall in shear- and pressure-driven flows," J. Fluid Mech. **383**, 29 (1999).
[11] S. Yon and C. Pozrikidis, "Deformation of a liquid drop adhering to a plane wall: Significance of the drop viscosity and the effect of an insoluble surfactant," Phys. Fluids **11**, 1297 (1999).
[12] P. D. M. Spelt, "Shear flow past two-dimensional droplets pinned or moving on an adhering channel wall at moderate Reynolds numbers: A numerical study," J. Fluid Mech. **561**, 439 (2006).
[13] E. B. Dussan V. and R. T.-P. Chow, "On the ability of drops or bubbles to stick to non-horizontal surfaces of solids," J. Fluid Mech. **137**, 1 (1983).
[14] E. B. Dussan V. "On the ability of drops or bubbles to stick to non-horizontal surfaces of solids. Part 2. Small drops or bubbles having contact angles of arbitrary size," J. Fluid Mech. **151**, 1 (1985).
[15] E. B. Dussan V. "On the ability of drops to stick to surfaces of solids. Part 3. The influences of the motion of the surrounding fluid on dislodging drops," J. Fluid Mech. **174**, 381 (1987).
[16] P. Dimitrakopoulos and J. J. L. Higdon, "On the gravitational displacement of three-dimensional fluid droplets from inclined solid surfaces," J. Fluid Mech. **395**, 181 (1999).
[17] P. Dimitrakopoulos and J. J. L. Higdon, "On the displacement of three-dimensional fluid droplets adhering to a plane wall in viscous pressure-driven flows," J. Fluid Mech. **435**, 327 (2001).
[18] P. Dimitrakopoulos and J. J. L. Higdon, "On the displacement of three-dimensional fluid bridges from solid surfaces in viscous pressure-driven flows," Phys. Fluids **15**, 3255 (2003).
[19] Q. J. Kang, D. X. Zhang, and S. Y. Chen, "Displacement of a three-dimensional immiscible droplet in a duct," J. Fluid Mech. **545**, 41 (2005).
[20] J. Zhang, M. J. Miksis, and S. G. Bankoff, "Nonlinear dynamics of a two-dimensional viscous drop under shear flow," Phys. Fluids **18**, 072106 (2006).
[21] P. Dimitrakopoulos, "Interfacial dynamics in Stokes flow via a three-dimensional fully-implicit interfacial spectral boundary element algorithm," J. Comput. Phys. **225**, 408 (2007).
[22] G. P. Muldowney and J. J. L. Higdon, "A spectral boundary element approach to three-dimensional Stokes flow," J. Fluid Mech. **298**, 167 (1995).
[23] T. Podgorski, J.-M. Flesselles, and L. Limat, "Corners, cusps, and pearls in running drops," Phys. Rev. Lett. **87**, 036102 (2001).